JOURNAL OF CATALYSIS 144, 611–626 (1993)

Influence of Hydrogen Pretreatment on the Structure of the Metal-Support Interface in Pt/Zeolite Catalysts

M. VAARKAMP,* F. S. MODICA,† J. T. MILLER,† AND D. C. KONINGSBERGER‡[1]

*Schuit Institute of Catalysis, Eindhoven University of Technology, P.O. Box 513, 5600 MB Eindhoven, The Netherlands; †Amoco Oil Company, Amoco Research Center, 150 West Warrenville Rd., Naperville, Illinois, 60566-7011; and ‡Department of Inorganic Chemistry, Debye Institute, Utrecht University, P.O. Box 80083, 3508 TB Utrecht, The Netherlands

Received April 8, 1993; revised July 26, 1993

Platinum supported on H-LTL, K-LTL, and H-MAZ was reduced at temperatures from 573 to 873 K and the structure of the metal-support interface was determined by EXAFS. In all samples, the platinum was highly dispersed, with metal particle sizes from 5–11 atoms. After low temperature reduction (LTR, 573 K), the distance between the platinum atoms and the oxide atoms of the support (Pt–O distance) is 2.7 Å, which is significantly longer than the Pt–O distance of 2.2 Å observed after high temperature reduction (HTR, 873 K). At intermediate reduction temperatures both the long and the short Pt–O distances are observed. The shortening of the Pt–O distance, combined with the decrease in both the Debye–Waller factor and the inner potential shift, implies a stronger interaction between the platinum atoms and the oxide support. A structural model is proposed wherein the longer Pt–O distance results from the presence of hydrogen in the interfacial layer between the metal particle and the support. During high temperature reduction, the hydrogen is released from the interface, leaving platinum in direct contact with the support. The shortening of the Pt–O interfacial distance is accompanied by a decrease in the hydrogen chemisorption capacity, and may additionally be related to changes in the catalytic properties.

INTRODUCTION

A number of studies have appeared in the literature using EXAFS to investigate the structure of supported noble metal catalysts. In the early studies, only the structural properties of the metal particle were characterized (*1–3*). Because the metal particles were relatively large, the fraction of metal atoms at the metal-support interface was small, and accurate information about the interface could not be obtained. Later studies indicated that the metal particle is supported directly on the oxide surface with reported metal-oxygen distances between 1.92 and 2.07 Å for platinum on alumina (*4*), platinum on silica (*5*), and rhodium on magnesia (*6*). These distances approximate the known metal–oxygen bond lengths in metal oxide compounds, and are about equal to the sum of the covalent radii of the metal and oxygen atoms. However, even in these later studies, the metal particles were still larger than about 15 atoms ($N \geq 6$), limiting the accuracy with which the metal-support distance could be determined. With very small Ir particles on alumina ($N = 4$), a longer Ir–O distance of 2.19 Å was observed after evacuation at 623 K (*7*).

In contrast, longer metal–oxygen distances (ca. 2.7 Å) have been reported for rhodium (*8–19*), iridium (*11*), and platinum (*12*) on alumina, iridium, on magnesia (*13*), palladium (*14*) and platinum (*15*) in zeolites, and rhodium on titania (*16*). For Rh/alumina (*9*) the Rh–O contribution increased as the metal particle size decreased, indicating that this Rh–O contribution arises from the interface between the rhodium and the oxide sup-

[1] To whom correspondence should be addressed.

0021-9517/93 $5.00

port. The lengthening of the metal-oxygen distance has been suggested to be due to the presence of hydrogen or OH groups in the metal-support interface (*7*). However, a clear understanding of the longer metal–oxygen distance is still lacking (*17*).

The present study utilized X-ray absorption spectroscopy to determine the effect of reduction temperature on the structure of the metal-support interface for small platinum clusters on H-LTL, K-LTL and H-MAZ zeolites. We have also established the experimental conditions which lead to the formation of the long and short metal–oxygen distance. The structural changes in the metal-support interface are discussed in relation to changes in hydrogen chemisorption capacity and catalytic properties reported in the literature.

EXPERIMENTAL

Preparation of Catalysts

The K-LTL zeolite was obtained from Linde. The zeolite was repeatedly washed with water until the pH of the wash solution was 9.5. The resulting K-LTL zeolite was analyzed to contain 8.3 wt% Al and 13.0 wt% K. The H-LTL zeolite was prepared by ion-exchanging the as-received K-LTL with ammonium nitrate solution at 363 K. The resulting exchanged zeolite contained 5.6 wt% K. The H-MAZ was prepared from Na-MAZ, which was synthesized following published procedures (*18*). The Na-MAZ was ion-exchanged with ammonium nitrate at 363 K. The resulting exchanged zeolite contained 0.01 wt% Na. All three zeolites were dried and calcined at 700 K.

The zeolites were impregnated with tetraamine platinum (II) nitrate to yield 1.2 wt% Pt on the finished catalyst. The impregnated catalysts were dried at 400 K.

Hydrogen Chemisorption

Volumetric hydrogen chemisorption measurements were performed in a conventional glass system at 298 K. Hydrogen was dried by passage over silica. Before measurement of the chemisorption isotherm, the catalyst samples were rereduced for 1 hr (heating rate 5 K/min) at 573, 723, or 873 K and evacuated (10^{-2} Pa) for 10 min at 473 K. After hydrogen admission at 473 K (pressure = 93 kPa), desorption isotherms were measured at room temperature. The amount of chemisorbed H_2 was obtained by linear extrapolation of the high-pressure part of the isotherm to zero pressure. Details are given elsewhere (*19*).

EXAFS Data Collection

The samples were characterized by EXAFS spectroscopy at the Synchrotron Radiation Source in Daresbury, U.K. Wiggler Station 9.2, using a Si (220) double crystal monochromator. The storage ring was operated with an electron energy of 2 GeV and a current between 120 and 250 mA. At the Pt L_{III} edge (11564 eV), the estimated resolution was 3 eV. The monochromator was detuned to 50% intensity to avoid the effects of higher harmonics present in the X-ray beam. The measurements were done in the transmission mode. To decrease low- and high-frequency noise as much as possible, each data point was counted for 1 sec and 6 scans were averaged.

The samples were pressed into self-supporting wafers (calculated to have an absorbance of 2.5) and placed in a controlled-atmosphere cell (*20*). The samples were reduced *in situ* in flowing hydrogen (purified and dried) at 1 atm. Samples were heated at 5 K/min to the desired reduction temperature (Pt/H-LTL: 573 and 773 K; Pt/K-LTL: 573, 723, and 873 K; Pt/H-MAZ: 723 K) and each was reduced for 1 hr. The samples were cooled to room temperature under flowing hydrogen. The measurements were done with the sample at liquid nitrogen temperature in the presence of hydrogen at atmospheric pressure.

EXAFS Data Analysis

Data reduction. The preedge background was approximated by a modified Victoreen curve (*21*), and the background was subtracted using cubic spline routines (*22*).

Spectra were normalized by dividing the absorption intensity by the height of the absorption edge at 50 eV above the edge. The final EXAFS function was obtained by averaging the individual background-subtracted and normalized EXAFS data (6 scans). The standard deviations over the six scans were calculated for each individual EXAFS data point as a measure of the random error in the final EXAFS function. The EXAFS data analysis is usually performed on an isolated part of the data obtained by an inverse Fourier transformation over a selected range in *r*-space. The isolated EXAFS functions were obtained by averaging the inverse Fourier transformations of each individual EXAFS data set (6 scans). The standard deviation of each data point, calculated from the six isolated EXAFS functions, provided a measure of the random error in the average isolated EXAFS function.

Reference data. Data for the phase shifts and backscattering amplitudes were obtained from EXAFS data obtained from reference compounds. Pt foil was used as a reference for the Pt–Pt contributions and $Na_2Pt(OH)_6$ for the Pt–O contributions. The procedures used to obtain the reference data for Pt foil and $Na_2Pt(OH)_6$ are described elsewhere (*23*).

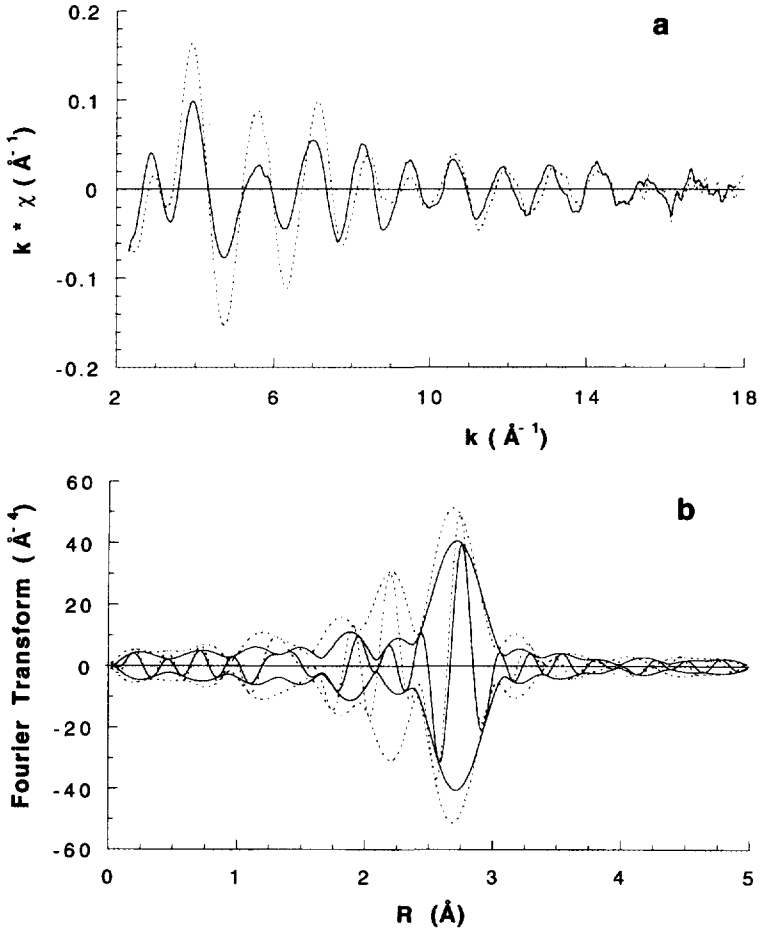

FIG. 1. (a) EXAFS spectra (k^1 weighted) of Pt/H-LTL reduced at 573 K (solid line) and 773 K (dotted line), (b) Fourier transform (k^3, Δk: 2.6–13.9 $Å^{-1}$, Pt–Pt phase and amplitude corrected) of the spectra in (a).

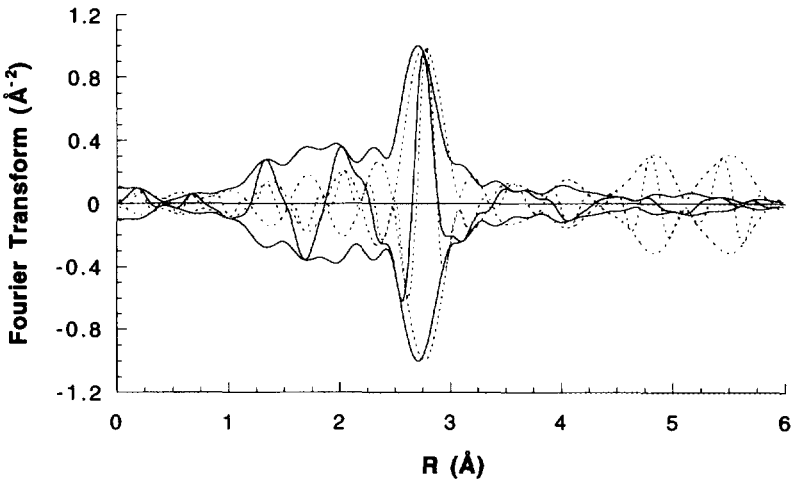

FIG. 2. Normalized Fourier transform of Pt/H-LTL reduced at 573 K (solid line) and Pt foil (dotted line) (k^1, Δk: 3.1–13.9 Å^{-1}, Pt–Pt phase- and amplitude-corrected).

Data analysis. The parameters characterizing the high-Z (Pt) and low-Z (O) contributions were determined by multiple-shell fitting in k-space with optimization in r-space. Different backscatterers were identified by applying the difference file technique using phase- and amplitude-corrected Fourier transforms (*5, 9, 16*). The optimal combination of the coordination number and the Debye–Waller factor was determined by optimizing the k^1 and k^3 weighted Fourier transforms (*23*). The statistical error in the structural parameters was calculated from the covariance matrix, taking into account the statistical noise obtained for the Fourier filtered EXAFS function and the correlations between the refined parameters (*24*). The values of the goodness of fit (ε_ν^2) were calculated as outlined in the *Report on Standards and Criteria in XAFS Spectroscopy* (*25*).

RESULTS

EXAFS Analysis of Pt/H-LTL

The EXAFS data (average of 6 scans) for Pt/H-LTL reduced at 573 K (LTR) and 773 K (HTR) are shown in Figure 1a. At low k values the amplitude of the EXAFS function is higher after reduction at 773 K than after reduction at 573 K. In addition, the position of the nodes in the EXAFS function are located at different k values. For the sample reduced at 573 K, the calculated signal-to-noise ratio is 15 at k = 4 Å^{-1} and 5 at k = 14 Å^{-1}. For the sample reduced at 773 K, the signal-to-noise was 60 and 5 at the same k values. Fourier transforms (k^3 weighted, Pt–Pt phase- and amplitude-corrected) of the EXAFS data for the Pt/H-LTL catalysts are shown in Fig. 1b. The Fourier transforms show an increase in the Pt–Pt contribution around 2.7 Å, indicating a growth in the Pt particle at higher reduction temperature. Furthermore, for Pt/H-LTL reduced at 773 K, an additional scatterer besides platinum is visible as a separate peak near 2.2 Å in the Fourier transform. This peak results from an interference which is observable in the raw EXAFS spectrum (Figure 1a) by the presence of a beating node at k = 9–10 Å^{-1}.

The normalized k^1 weighted Fourier transforms (Pt–Pt phase- and amplitude-corrected) of the EXAFS data for Pt/H-LTL reduced at 573 K and for Pt foil are shown in Fig. 2. The Fourier transforms are normalized to facilitate comparison and k^1 weighted in order to emphasize the low-Z (oxygen) contributions. Differences are observed between the Pt/H-LTL catalyst and

TABLE 1

Structural Parameters from EXAFS for Pt/H-LTL after Reduction at 573 and 773 K

Backscatterer	T_{red} (K)	N	R(Å)	$\Delta\sigma^2$ (Å^2 × 10^{-3})	ΔE_0 (eV)
Pt	573	4.1 ± 0.1	2.73 ± 0.01	3.4 ± 0.1	3.5 ± 0.3
	773	4.4 ± 0.1	2.72 ± 0.01	4.4 ± 0.1	0.8 ± 0.2
O	573	1.2 ± 0.1	2.65 ± 0.01	7.0 ± 1.1	5.7 ± 0.5
	773	1.5 ± 0.1	2.24 ± 0.01	−2.5 ± 1.1	−13.9 ± 0.1

the Pt foil in both the magnitude and the imaginary part of the Fourier transforms between 2.0–3.5 Å. These differences indicate the presence of additional scatterers besides Pt in the Pt/H-LTL catalyst. Multiple-shell fitting of the Fourier-filtered EXAFS spectrum (k^2, Δk: 2.6–13.9 Å^{-1}, ΔR: 1.2–3.3 Å) resulted in the identification of two significant contributions (Table 1): a Pt–Pt contribution at 2.73 Å with a coordination number of 4.1 (ca. 6 Pt atoms/cluster) and a Pt–O contribution from the zeolite framework at 2.65 Å and a coordination number of 1.2. The goodness of fit (*25*) was calculated to be 21.8 with eight fit parameters and 13.7 degrees of freedom. The Pt–O contribution was statistically significant at the 88% confidence level ($F = 2.51$). The Pt–O distance of 2.65 Å for this catalyst is in the same range as those previously observed for other supported metal catalysts reduced at low temperatures (*8–16*).

The results of the multiple-shell fitting of the Fourier-filtered (k^2, Δk: 2.8–13.9 Å^{-1}, ΔR: 1.15–3.25 Å) EXAFS data for the Pt/H-LTL reduced at 773 K are also given in Table 1. The Pt–Pt coordination number of 4.4 indicates a small increase in the platinum particle size to approximately 9 atoms. The Pt–O coordination number was 1.5. The goodness of fit (*25*) was calculated to be 38.7 with eight fit parameters and 13.7 degrees of freedom (Table 3). The Pt–O contribution at 2.65 Å, which was present after reduction at 573 K, disappears after reduction at 773 K, with the concurrent formation of the Pt–O contribution at 2.24 Å.

Subtraction of the calculated Pt–Pt contribution from the raw EXAFS spectrum results in a difference spectrum containing only contributions from the support. The Fourier transform (k^1 weighted, Pt–O phase-corrected) of this difference spectrum and the calculated Pt–O contribution is shown for Pt/H-LTL reduced at 573 K (Fig. 3a) and 773 K (Fig. 3b). The different Pt–O distances in the two catalysts can be clearly seen. Reduction at 573 K results in a Pt–O distance of 2.65 Å, while reduction at 773 K results in a Pt–O distance of 2.24 Å. The peak associated with the longer Pt–O distance is significantly broader than that associated with the shorter Pt–O distance. The broader peak is an indication of a larger deviation about the mean distance, i.e., a larger Debye–Waller factor ($\Delta\sigma^2$). In addition to the difference in the Debye–Waller factor, the two platinum–oxygen contributions also have different inner potential shifts (ΔE_0) (see Table 1). These changes are indicative of a strengthening of the interaction between the platinum clusters and the oxide support during HTR.

EXAFS Analysis of Pt/K-LTL

In general, the structure of the Pt-support interface in Pt/K-LTL and the effects of reduction temperature are similar to those observed for Pt/H-LTL. The increase in the amplitude of the EXAFS function at low k and the shift in the position of the nodes with increasing reduction temperature (Fig. 4a), indicate the growth of the platinum particles and a change in the structure of the metal-support interface. Fourier transforms show a peak developing at around 2.2 Å as

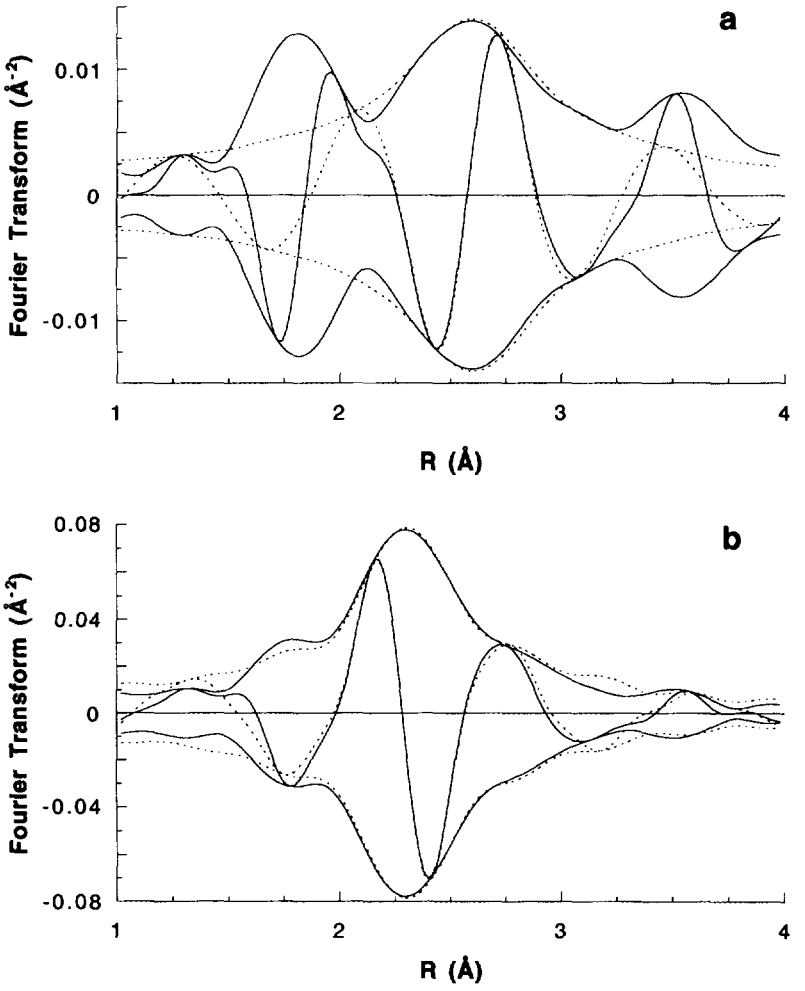

FIG. 3. Fourier transform (k^1, Δk: 3.5–12.0 Å^{-1}, Pt–O phase-corrected) of the EXAFS spectrum of Pt/H-LTL minus the Pt–Pt contribution (solid line) and the Pt–O contribution calculated with the parameters in Table 1 (dotted line). (a) reduced at 573 K, (b) reduced at 773 K.

the reduction temperature is increased (Fig. 4b). Full fitting of the EXAFS data for the Pt/K-LTL catalysts results in the coordination parameters given in Table 2. The spectra calculated with the refined parameters, are compared with the Fourier-filtered EXAFS spectra in Fig. 5. After reduction at 573 K, the Pt–Pt coordination number is 4.0, i.e., a Pt cluster of 6 atoms, and only the long (2.77 Å) Pt–O distance is present. After 873 K reduction the Pt–Pt coordination number increased to 4.9, or approximately 11 atoms, and only the shorter (2.24 Å) Pt–O distance is present. At the intermediate reduction temperature of 723 K, both Pt–O contributions are present. Thus, there appears to be a transformation from the long Pt–O distance (ca. 2.7 Å) to a short Pt–O distance (2.2 Å) with increasing reduction temperature.

Fourier transforms (k^1 weighted, Pt–O phase corrected) of the isolated Pt–O contributions and the calculated Pt–O contributions are presented in Fig. 6. As was ob-

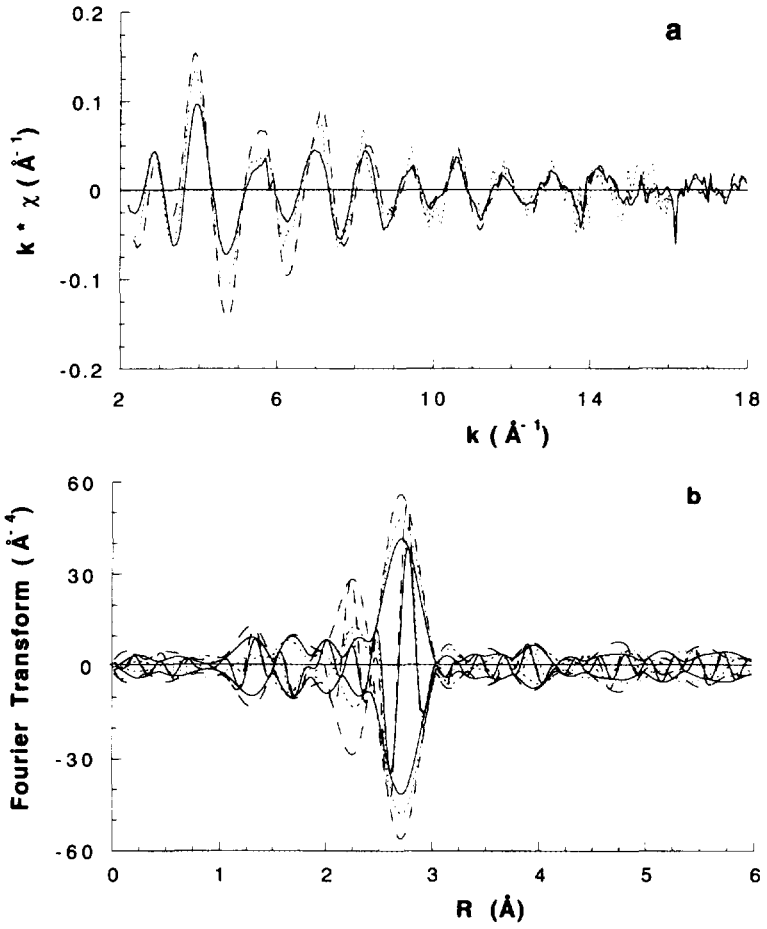

FIG. 4. EXAFS spectra (k^1 weighted) of Pt/K-LTL reduced at 573 K (solid line), 723 K (dotted line), and 873 K (dashed line). (b) Fourier transform (k^3, Δk: 3.1–15.0 Å^{-1}, Pt–Pt phase- and amplitude-corrected) of the spectra shown in (a).

TABLE 2

Structural Parameters from EXAFS for Pt/K-LTL after Reduction at 573, 723, and 873 K

Backscatterer	T_{red} (K)	N	R (Å)	$\Delta\sigma^2$ (Å^2 × 10^{-3})	ΔE_0 (eV)
Pt	573	4.0 ± 0.1	2.74 ± 0.01	4.4 ± 0.1	2.0 ± 0.3
	723	4.8 ± 0.2	2.74 ± 0.01	4.4	2.0 ± 1.3
	873	4.9 ± 0.1	2.75 ± 0.01	4.4 ± 0.1	−0.6 ± 0.2
O	573	1.4 ± 0.1	2.73 ± 0.01	8.0 ± 1.1	0.3 ± 0.6
	723	1.3 ± 0.2	2.77 ± 0.05	8.0	−2 ± 4
		0.4 ± 0.1	2.20 ± 0.02	−1.6	−9 ± 3
	873	1.3 ± 0.1	2.24 ± 0.01	−1.6 ± 0.1	−13.4 ± 0.2

Note. Parameters without error were fixed during the refinement.

TABLE 3

Fourier Filtering Ranges and Goodness of Fit (ε_ν^2) Values

Sample	T_{red} (K)	Fourier filtering		Δk_{anal} (Å^{-1})	ε_ν^2
		Δk (Å^{-1})	ΔR (Å)		
Pt/H-LTL	573	2.64–13.93	1.21–3.27	3.50–13.00	21.8
	773	2.79–13.98	1.15–3.25	3.50–13.00	38.7
Pt/K-LTL	573	2.57–13.90	1.60–3.26	3.50–13.00	27.3
	723	2.64–13.33	1.50–3.36	3.50–12.50	2.8
	873	2.72–13.94	1.17–3.27	3.50–13.00	17.4
Pt/H-MAZ	723	2.66–12.04	1.52–3.39	3.50–11.00	11.2

served for Pt/H-LTL, the peak associated with the longer Pt–O distance in Pt/K-LTL is broader than that associated with the shorter Pt–O distance, i.e., a larger Debye–Waller factor ($\Delta\sigma^2$). The two platinum–oxygen contributions also have different inner potential shifts (ΔE_0) (see Table 2). As with Pt/H-LTL, these changes are indicative of changes in the nature of the interaction between the platinum clusters and the oxide support after LTR and HTR.

The goodness of fit values for the Pt/K-LTL catalysts are given in Table 3. The low value for Pt/K-LTL reduced at 723 K results from a lower signal to noise ratio for this sample, which limited the usable data range to Δk = 3.5–12.5 Å^{-1}. This data range allows only 10.5 degrees of freedom, which is not large enough to justify the fitting of the twelve free parameters needed for three contributions. Therefore, we chose to fix the Debye–Waller factors for the Pt–Pt and Pt–O contributions at the values obtained for the Pt/K-LTL samples reduced at 523 K and 773 K. This decreased the number of fit parameters to nine, which is less than the 10.5 degrees of freedom calculated from the Nyquist theorem.

EXAFS Analysis of Pt/H-MAZ

The EXAFS data (average of 6 scans) for Pt/H-MAZ reduced at 723 K are shown in Figure 7a. Because of the low signal to noise ratio of the data, analysis was only possible up to k = 11 Å^{-1}. Analysis of the Fourier-filtered data (Table 4) shows that besides the Pt–Pt contribution, a Pt–O contribution at a distance of 2.2 Å is present. The Pt–Pt coordination number of 2.9 indicates an average particle size of 4 atoms. These results are similar to those observed for Pt/K-LTL and Pt/H-LTL after HTR. The negative Debye–Waller factor and the large negative value of −10 eV for the inner potential shift for this Pt–O contribution are also similar to those observed for both Pt/LTL catalysts after HTR. These very low values suggest that oxygen might not be the correct backscatterer for this contribution. While K-LTL and even H-LTL contain significant amounts of potassium, H-MAZ contains no potassium and only 100 ppm Na. Therefore, the contribution at 2.2 Å cannot be due to backscattering by potassium. The only other possible backscatterers in H-MAZ are aluminum and silicon. Fitting of the EXAFS spectrum using a Pt–Al absorber–backscatterer pair resulted in a poorer fit than was obtained with the Pt–O absorber–backscatterer pair (ε_ν^2 = 11.2 vs 17.3, respectively). Taken together, these results indicate that oxygen is the correct backscatterer, and that the large negative values in the Debye–Waller factor and the inner potential shift for the 2.2 Å Pt–O contribution indicate a stronger interaction between the platinum and the oxide support compared to the 2.7 Å Pt–O contribution.

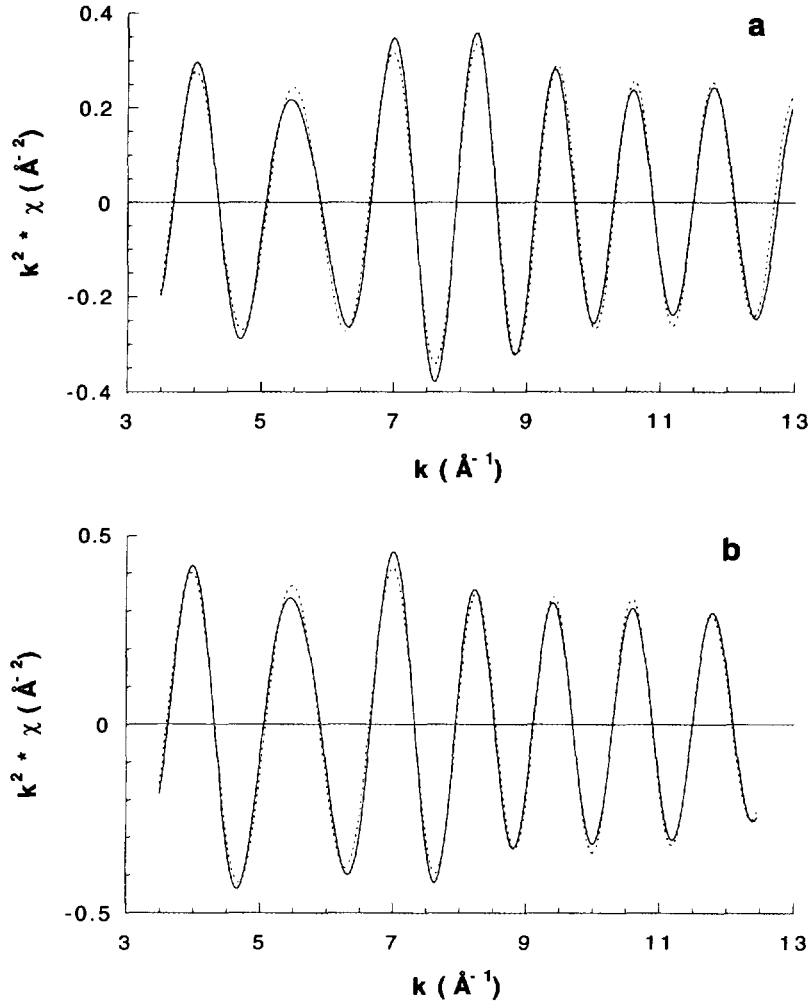

FIG. 5. Results of EXAFS analysis of Pt/K-LTL reduced at (a) 573 K, (b) 723 K, and (c) 873 K, solid line Fourier filtered data, dotted line model EXAFS spectrum calculated with the parameters in Table 2. The Fourier transform (k^2, Δk: 3.5–13.0 $Å^{-1}$) of the spectra in (a), (b), and (c) are shown in (d), (e), and (f), respectively.

Hydrogen Chemisorption

The results of the hydrogen chemisorption measurements are shown in Table 5. The H/Pt values, which are all larger than 0.8, indicate that all catalysts contain highly dispersed platinum. Many of the H/Pt values are significantly greater than 1.0, indicating that platinum atoms in very small clusters are capable of chemisorbing more than one hydrogen atom (*19*). Figure 8 shows the relationship between the H/Pt and the reduction temperature. While increasing reduction temperature did result in some platinum particle growth, the largest particles are still quite small, with nearly all the platinum atoms at the surface. The decrease in hydrogen chemisorption with increasing reduction temperatures far exceeds this small loss in exposed platinum due to particle growth. This indicates a change in the chemistry of the platinum clusters resulting from a change in the structure of the metal-support

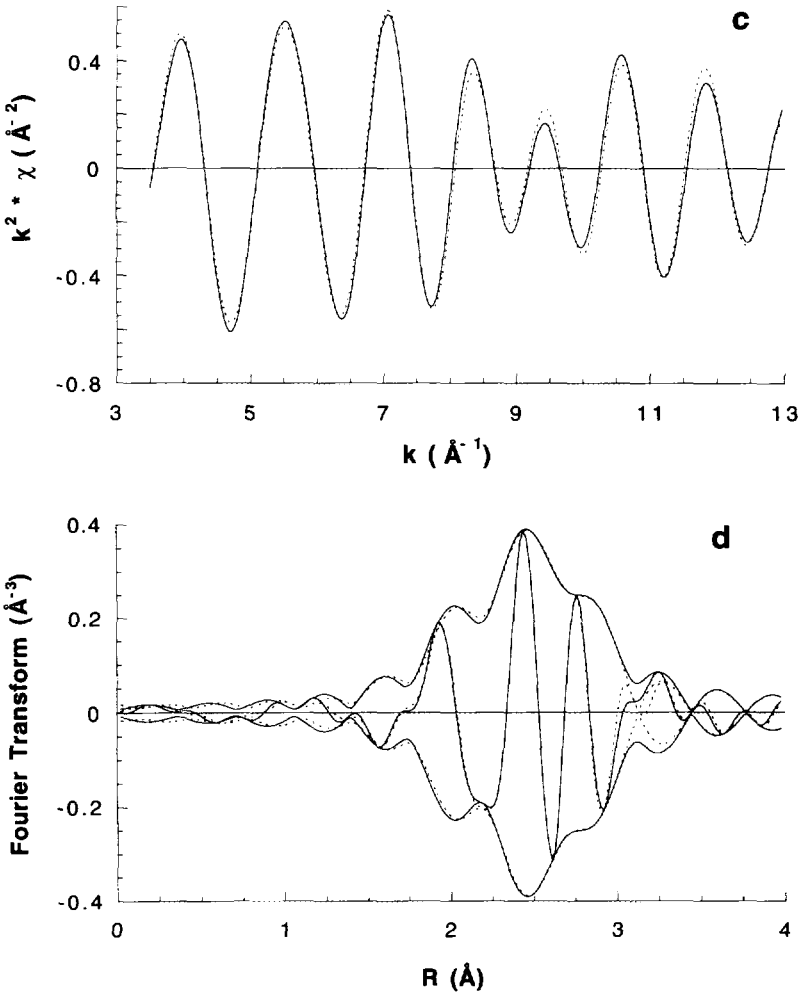

FIG. 5—(*Continued*)

interface, which is also consistent with the strengthening of the metal-support interaction implied by the EXAFS results.

DISCUSSION

Pt–Pt Distance

Due to the decreased delocalization of electrons in small metal particles a contraction of the Pt–Pt distance in the very small crystallites used in this study is expected (*30*). However, EXAFS experiments on platinum clusters in zeolite Y (*31*) and iridium clusters on γ-Al_2O_3) (*7*) with and without chemisorbed hydrogen have shown that the contraction (>0.1 Å) only occurs without chemisorbed hydrogen. Chemisorbed hydrogen apparently opposes the delocalization of electrons. The measurements reported in this paper were performed in a hydrogen atmosphere, hence, the found Pt–Pt distances near the bulk value of 2.77 Å are in agreement with these earlier measurements.

Short Pt–O Distance

The short Pt–O distance of 2.2 Å observed in this study is approximately equal to the sum of the covalent radii, and is char-

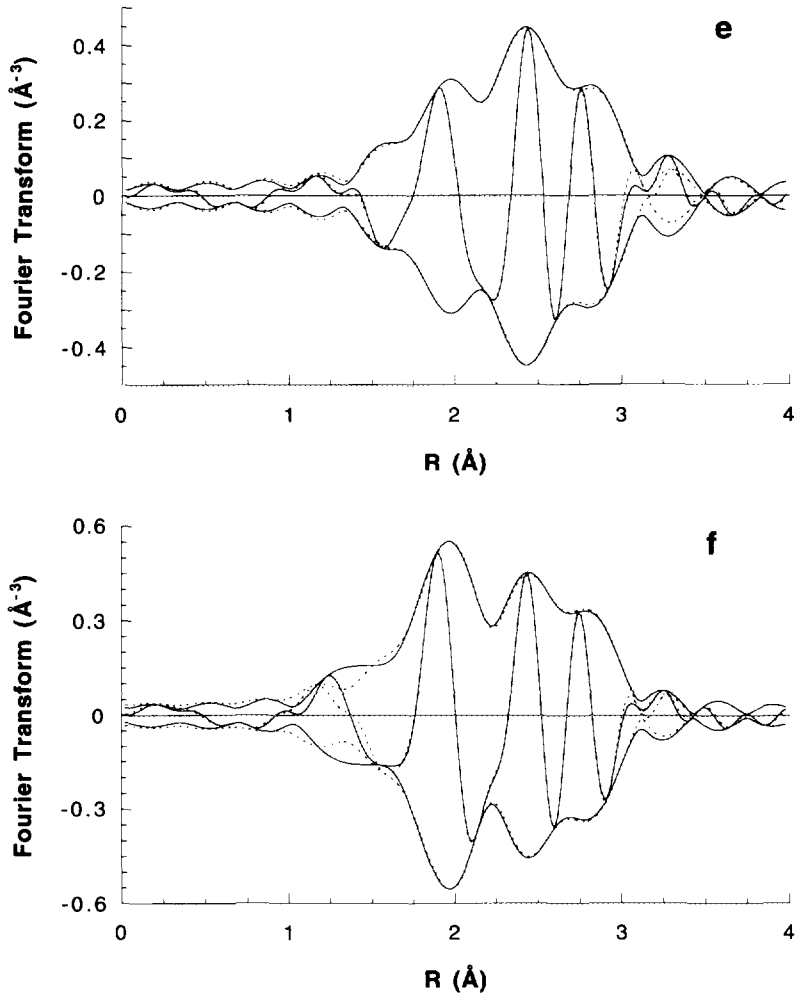

FIG. 5—(*Continued*)

acteristic of support oxygen atoms in contact with zero-valent metal clusters. Similar metal–oxygen distances were observed by EXAFS on reduced Ir/alumina after evacuation (2.19 Å) and after oxygen adsorption at 77 K (2.21 Å) (*7*). In addition, metal-oxygen bond lengths of 2.1–2.2 Å have been observed by EXAFS for low-valent, supported noble metal subcarbonyls (*26*) and by X-ray diffraction (XRD) for lower valent noble metal compounds containing oxygen ligands (*17*).

In contrast, metal–oxygen distances in higher valent metal oxides are found to be considerably shorter than the 2.2 Å found in the present study. For example, metal–oxygen bond distances of 2.05 Å have been determined by XRD for Rh_2O_3 (*27*) and $Na_2Pt(OH)_6$ (*28*). Similarly, Pt–O distances of 2.01–2.05 Å were found by EXAFS for Pt^{+2}-exchanged zeolite Y (*15*). Further, oxygen chemisorption at 298 K on prereduced Pt/SiO_2 leads to a Pt–O distance of 2.03 Å (*5*), which is shorter than the distance observed after oxygen adsorption at 77 K (2.21 Å) (*7*). The shorter (2.03 Å) distance after 298 K chemisorption is in the range expected for oxidic platinum, and may

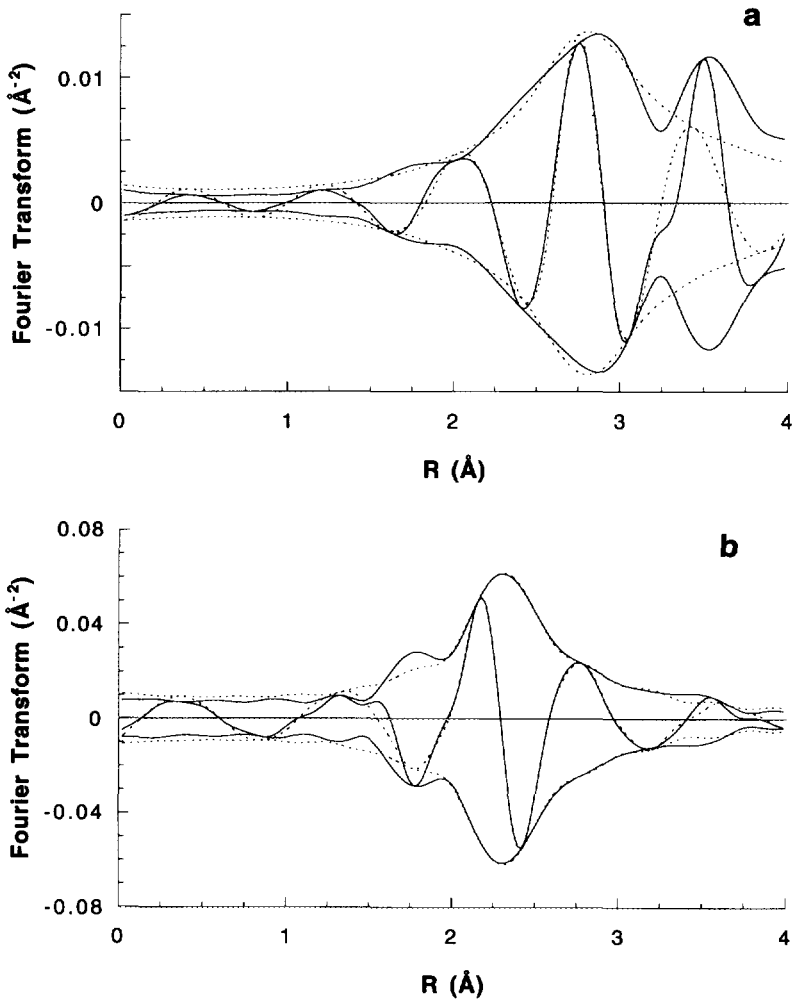

FIG. 6. Fourier transform (k^1, Δk: 3.5–12.0 Å^{-1}, Pt–O phase-corrected) of the EXAFS spectrum of Pt/K-LTL minus the Pt–Pt contribution (solid line) and the Pt–O contribution calculated with the parameters in Table 2 (dotted line). (a) reduced at 573 K, (b) reduced at 873 K.

suggest oxidation of at least the surface metal atoms under these conditions.

In a few early studies of reduced supported metal catalysts, metal–oxygen distances of 1.92–2.07 Å were reported (*4–6*), which are shorter than the 2.2 Å found in the present study. In the present study we used $Na_2Pt(OH)_6$ as reference for the Pt–O absorber–backscatterer pair, which is more reliable than the β-PtO_2 which was used in the earlier studies (*32*). In addition, the contribution to the total EXAFS signal arising from the metal-support interface is proportionally larger in the present study due to the much smaller metal particle size, i.e., larger Pt–O coordination number and smaller Pt–Pt coordination number. Finally, signal-to-noise ratios in the EXAFS data are much improved using current generation synchrotrons. These factors allow a more accurate determination of the structure of the metal-support interface.

Long Pt–O Distance

In the present study, we have shown that Pt–O distances of 2.6–2.7 Å are observed

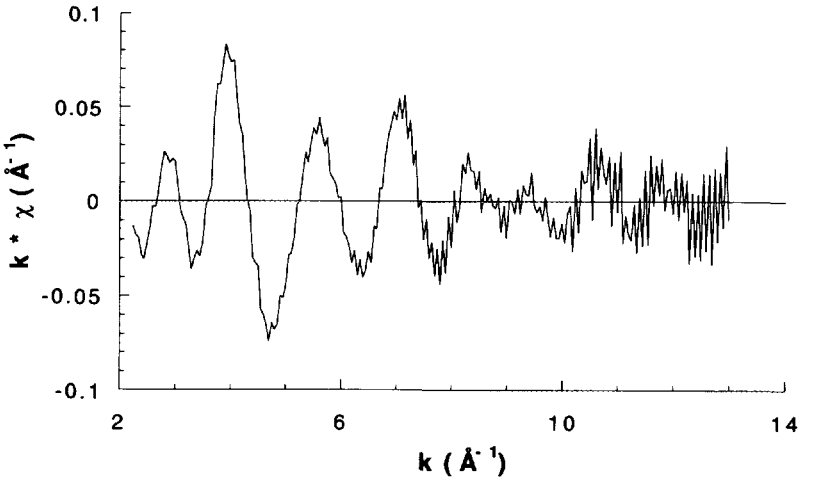

FIG. 7. EXAFS spectrum (k^1 weighted) of Pt/H-MAZ.

after LTR (≤573 K). Previous studies have also reported similar long metal–oxygen distances after LTR (*8–17*). This Pt–O distance is significantly longer than the 2.2 Å which is characteristic of zero-valent platinum in contact with an oxide support, and suggests the presence of an additional atom residing at the interface between the metal atoms and the support (*7*). The lack of observable backscattering from this atom in the EXAFS spectrum indicates that this interfacial atom must be a light atom, most likely hydrogen.

Structural Model of the Metal-Support Interface

In the conventional understanding of the structure of the interface between the metal and the support, the metal atoms are in direct contact with the oxide ions of the support. This model is consistent with the metal–oxygen distance of 2.2 Å, which is approximately equal to the sum of the covalent radii of the metal and oxygen atoms. By contrast, a longer metal–oxygen distance of ca. 2.7 Å is found after LTR. We propose that this longer Pt–O distance is a result of hydrogen in the metal-support interface. This is shown schematically in Fig. 9. During high temperature treatment, the interfacial hydrogen is removed as H_2, and this hydrogen desorption has been detected by H_2-TPD as peaks around 600–700 K (*33, 34*). Loss of interfacial hydrogen results in a shortening of the Pt–O distance to 2.2 Å. This process is complete above about 750 K, but may be incomplete at lower temperatures, leaving some platinum atoms in contact with the interfacial hydrogen while others are in direct contact with the oxide support.

While the interfacial hydrogen is removed during HTR, it is not reintroduced during cooling in hydrogen, indicating that the removal of hydrogen is irreversible. This lack

TABLE 4

Structural Parameters from EXAFS for Pt/H-MAZ after Reduction at 723 K

Backscatterer	N	R (Å)	$\Delta\sigma^2$ (Å^2 × 10^{-3})	ΔE_0 (eV)
Pt	2.9 ± 0.2	2.75 ± 0.01	6.0 ± 0.4	−1.7 ± 0.5
O	0.6 ± 0.1	2.23 ± 0.01	−3.0 ± 0.5	−12.2 ± 0.6

TABLE 5

Hydrogen Chemisorption Results

Sample	T_{red} (K)	H/Pt
Pt/H-LTL	573	1.70
	773	1.05
Pt/K-LTL	573	1.42
	723	1.27
	873	0.84
Pt/H-MAZ	723	1.15

of reversibility is also consistent with the stronger metal-support interaction indicated by the low values observed for the Debye–Waller factor and inner potential shift.

Previous studies of interfacial hydrogen were unable to distinguish whether the hydrogen was present as protonic hydrogen (as from support hydroxyl groups) or neutral atomic species (spilled over from the metal) (*7*). We suggest that the following observations are more consistent with the latter interpretation:

(1) After LTR of Ir/Al_2O_3 the observed Ir–O distance was 2.55 Å (*35*), but decreased to 2.19 Å following evacuation at 623 K (*7*). Although evacuation at these mild temperatures was able to remove the interfacial hydrogen, a significant amount of dehydroxylation seems unlikely.

(2) A long Ir–O distance was also observed for Ir/MgO (*13*), even though the support was thoroughly dehydroxylated prior to addition of the Ir.

(3) Liberation of interfacial hydrogen (as H_2) in the TPD was not accompanied by oxidation of the platinum (*36*), as would be expected if protonic hydrogen was reduced to form H_2.

These three observations indicate that the interfacial hydrogen is more likely atomic in nature, and similar in character to chemisorbed hydrogen. We suggest that this interfacial hydrogen is introduced during the reduction step, by the spillover of hydrogen from the metal.

Implications for Catalysis

The low Debye–Waller factor and inner potential shift found after HTR are consistent with a strengthening of the metal-support interaction. This results in a change in the chemistry of the supported platinum cluster as evidenced by the decrease in hydrogen chemisorption capacity. A similar loss in H_2 chemisorption capacity after HTR was reported in a recent study of Pt/SiO_2

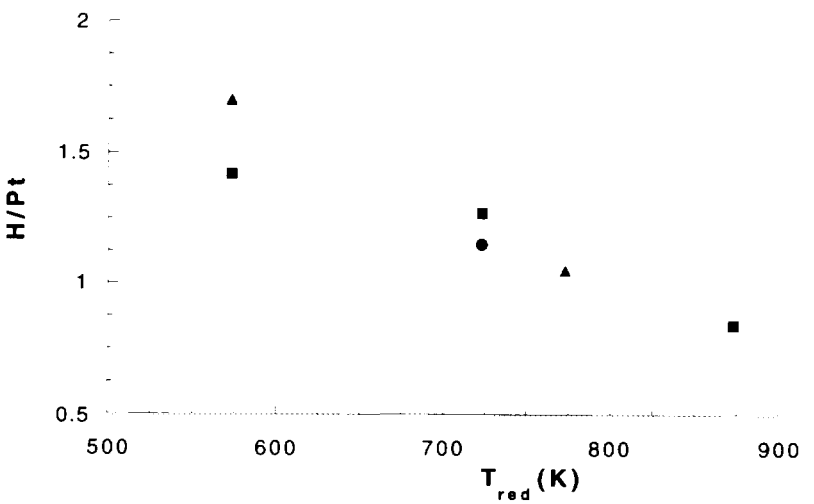

FIG. 8. Amount of hydrogen chemisorbed per platinum atom as a function of reduction temperature, triangle: Pt/H-LTL, square: Pt/K-LTL, and circle: Pt/H-MAZ.

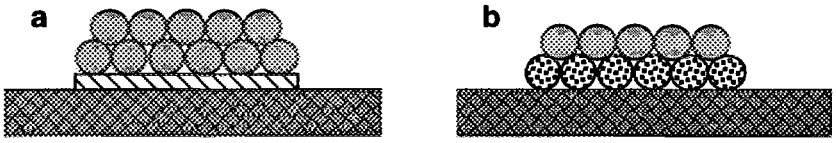

FIG. 9. Schematic representation of the changes in the structure of the metal-support interface as a function of the reduction temperature, (a) LTR: hydrogen present in the metal-support interface, (b) HTR: interfacial platinum atoms in direct contact with support.

(*37*). Changes in catalytic activity and selectivity resulting from high temperature reduction have also been reported. High temperature reduction has been shown to suppress hydrogenolysis activity with a variety of reactants and catalysts: *n*-pentane over Pt on Al_2O_3, SiO_2, and TiO_2 (*38*), ethane over Ru on SiO_2 (*39*), propane over Pt in zeolites (*29*), and methylcyclopentane ring opening over Pt on SiO_2 and Al_2O_3 (*40*). High temperature reduction can also affect the selectivity of the reaction. For example, for MCP ring opening over Pt on SiO_2 and on Al_2O_3, high temperature reduction decreased the selectivity to *n*-hexane (*40*), while for Pt on SiO_2 and Y zeolites, the ratio of isomerization to hydrogenolysis of neopentane decreased with increasing reduction temperature (*41*).

In the present study, we have shown that high temperature reduction leads to structural changes in the metal-support interface. At high reduction temperatures, hydrogen is lost from the metal-support interface, leaving the metal particles in direct contact with the oxide ions of the support. While the details of how these structural changes affect the catalytic and chemisorptive properties are not yet understood, the observed changes in the Debye–Waller factor and inner potential shift are strong indications of a change in the electronic properties of the metal, which may be responsible for at least some of the changes in catalytic and chemisorptive properties observed.

CONCLUSIONS

The extremely small metal particles of 5–11 atoms present in these LTL zeolite catalysts allow for an accurate characterization of the structure of the metal-support interface by EXAFS. Low temperature reduction (LTR, 573 K) leads to the formation of a long Pt–O distance (ca. 2.7 Å). In contrast, high temperature reduction (HTR, 873 K) leads to the formation of a shorter Pt–O distance (ca. 2.2 Å). At intermediate temperatures, both Pt–O distances are observed. It is proposed that the long Pt–O distance is due to the presence of spilled-over hydrogen in the interface between the platinum atoms and the oxide surface. This interfacial hydrogen is lost during high temperature reduction, leaving the platinum atoms in direct contact with the oxide surface. This results in a stronger metal-support interaction, which affects the chemistry of the platinum clusters, reducing the chemisorptive capacity and influencing catalytic activity and selectivity for a variety of reactions. The details of this metal-support interaction and how it affects the catalytic and chemisorptive properties of the metal are not yet understood, and this will be the subject of future investigations.

REFERENCES

1. Sinfelt, J. H., Via, G. H., and Lytle, F. W., *J. Chem. Phys.* **68,** 2009 (1978).
2. Lytle, F. W., Wei, P. S. P., Greegor, R. B., Via G. H., and Sinfelt, J. H., *J. Chem. Phys.***70,** 4849 (1979).
3. Via, G. H., Sinfelt, J. H., and Lytle, F. W., *J. Chem. Phys.* **71,** 690 (1979).
4. Lagarde, P., Murata, T., Vlaic, G., Freund, E., Dexpert H., and Bournonville, J. P., *J. Catal.* **84,** 333 (1983).
5. Lytle, F. W., Greegor, R. B., Marques, E. L., Sanstrom, D. R., Via, G. H., and Sinfelt, J. H., *J. Catal.* **95,** 546 (1985).

6. Emrich, R. J., Mansour, A. N., Sayers, D. E., McMillan, S. T. and Katzer, J. R., *J. Phys. Chem.* **89,** 4261 (1985).
7. Kampers, F. W. H., and Koningsberger, D. C., *Faraday Disc. Chem. Soc.* **89,** 137 (1990).
8. van't Blik, H. F. J., van Zon, J. B. A. D., Huizinga, H. F., Vis, J. C., Koningsberger, D. C., and Prins, R., *J. Am. Chem. Soc.* **107,** 3139 (1985).
9. van Zon, J. B. A. D., Koningsberger, D. C., van't Blik, H. F. J., and Sayers, D. E., *J. Chem. Phys.* **12,** 5742 (1985).
10. Koningsberger, D. C., van Zon, J. B. A. D., van't Blik, H. F. J., Visser, G. J., Prins, R., Mansour, A. N., Sayers, D. E., Short D. R., and Katzer, J. R., *J. Chem. Phys.* **89,** 4075 (1985).
11. van Zon, F. B. M., Visser, G., and Koningsberger, D. C., *in* "Proc. 9th Int. Cong. Catal" (J. J. Phillips and M. Ternan, Eds.). Vol. 3, p. 1386. Chemical Institute of Canada, Ottawa, 1988.
12. Koningsberger, D. C., and Sayers, D. E., *Solid State Ionics* **16,** 23 (1985).
13. van Zon, F. B. M., Maloney, S. D., Gates, B. C., and Koningsberger, D. C., *J. Am. Chem. Soc.*, in press.
14. Möller, K., Koningsberger, D. C., and Bein, T., *J. Phys. Chem.* **93,** 6116 (1989).
15. Tzou, M. S., Teo, B. K., and Sachtler, W. M. H., *J. Catal.* **113,** 220 (1988).
16. Martens, J. H. A., Prins, R., Zandbergen, H., and Koningsberger, D. C., *J. Phys. Chem.* **92,** 1903 (1988).
17. Koningsberger, D. C., and Gates, B. C., *Catal. Lett.* **14,** 271 (1992).
18. Breck, D. W., "Zeolite Molecular Sieves, Structure, Chemistry and Use," p. 306. Wiley, New York, 1974.
19. Kip, B. J., Duivenvoorden, F. B. M., Koningsberger, D. C., and Prins, R., *J. Catal.* **105,** 26 (1987).
20. Kampers, F. W. H., Maas, T. M. J., van Grondelle, J., Brinkgreve, P., and Koningsberger, D. C., *Rev. Sci. Instr.* **60,** 2645 (1989).
21. Vaarkamp, M., Dring, I., Oldman, R. J., Stern, E. A. and Koningsberger, D. C., submitted for publication.
22. Cook, J. W., Jr., and Sayers, D. E., *J. Appl. Phys.* **52,** 5024 (1981).
23. Kampers, F. W. H., Ph.D. thesis, Eindhoven University of Technology, Eindhoven, 1989.
24. Vaarkamp, M., Linders, J. C., and Koningsberger, D. C., in preparation.
25. Lytle, F. W., Sayers, D. E., and Stern, E. A., *Physica B* **158,** 701 (1989).
26. Chang, J. R., Gron, L. U., Honji, A., Sanchez, K. M., and Gates, B. C., *J. Phys. Chem.* **95,** 9944 (1991).
27. Coey, J. M., *Acta Crystallogr. Sect. B* **26,** 1876 (1970).
28. Trömel, M., and Lupprich, E.,*Z. Anorg. Chem.* **414,** 160 (1975).
29. Vaarkamp, M., Miller, J. T., Modica, F. S., Lane, G. S., and Koningsberger, D. C., *in* "New Frontiers in Catalysis. Proc. 10th Int. Congr. Catal., Budapest, July 19–24, 1992", (L. Guczi, F. Solymosi, and P. Tétényi, Eds.), p. 809, Elsevier, Amsterdam, 1993.
30. Gordon, M. B., Cyrot-Lackmann, F., and Desjonquères, M. C., *Surf. Sci.* **80,** 159 (1979).
31. Moraweck, B., Clugnet, G., and Renouprez, A. J., *Surf. Sci.* **81,** L631 (1979).
32. Mansour, A. N., Sayers, D. E., Cook, Jr., J. W., Short, D. R., Shannon, R. D., and Katzer, J. R., *J. Phys. Chem.* **88,** (1984) 1778.
33. Modica, F. S., Miller, J. T., Lane, G. S., Meyers, B. L., Vaarkamp, M., and Koningsberger, D. C., *Prep. ACS Petr. Div.* **37,** 1009 (1992).
34. Vaarkamp, M., van Grondelle, J., van Santen, R. A., Miller, J. T., Meyers, B. L., Modica, F. S., Lane, G. S., and Koningsberger, D. C., "Proc. 9th Int. Zeolite Conf. Montreal, July 5–10, 1992." Butterworth–Heinemann, London, Vol. II, p. 433 (1993).
35. van Zon, F. B. M., and Koningsberger, D. C., in preparation.
36. Miller, J. T., Meyers, B. L., Modica, F. S., Lane, G. S., Vaarkamp, M., and Koningsberger, D. C., *J. Catal.* **143,** 395 (1993).
37. Lamber, R., and Jaeger, N. I., *J. Appl. Phys.* **70,** 457 (1991).
38. Menon, P. G., and Froment, G. F., *Appl. Catal.* **1,** 31 (1981).
39. Guczi, L., Matusek, K., Manninger, I., Kiralay, J., and Eszterle, M., *in* "Proc. 2nd Inter. Symp. Scientific Bases for Prep. Het. Cat.", Louvain-la-Neuve, 1978. Elsevier, Amsterdam.
40. Kramer, R., and Fischbacher, M., *J. Mol. Catal.* **51,** 247 (1989).
41. Foger, K., and Anderson, J. R., *J. Catal.* **54,** 318 (1978).